Arch. Metall. Mater. **68** (2023), 4, 1357-1367

DOI: https://doi.org/10.24425/amm.2023.146201

C.B. DANISMAN[1], G. GOLLER[1*]

SPARK PLASMA SINTERED Mn-Al (MAGNETS) PRODUCTION AND CHARACTERIZATION WITH EXPERIMENTAL DESIGN

Mn-Al alloys are important alloys due to their magnetic properties and have been identified as permanent magnets. This alloy possesses magnetic properties and can be manufactured at a relatively low cost. Mn-Al alloys could be an alternative to rare earth magnets and hard ferrites and have a promising future. In this study, the effects of sintering temperature, holding time and pressure on densification, average grain size and magnetic properties of the SPS-ed Mn-Al alloys were observed. However, with the different sintering parameters, the magnetic phase τ phase could be achieved. To obtain the τ phase, different annealing methods were tried, yet samples heated to 650°C and air cooled exhibited magnetic properties. This sample was selected from various sintering parameters due to its high density of 99% N6 (800°C – 300 sec – 60 MPa) and has an average grain size of 137±18.1 μm. The uniqueness of this work is that statistical approaches such as Taguchi design of experiment (DOE) and regression were used for optimization of the manufacturing process.

Keywords: Mn-Al Magnets; SPS; τ phase; DOE

Highlights

- Mn-Al magnets were produced with the spark plasma technique.
- Samples with 99% relative density were obtained and crosschecked with an X-ray imaging device.
- The microstructures of the samples were investigated, and the average grain sizes were measured.
- Magnetic properties were evaluated with XRD phase analyses and verified with VSM analyses.
- The effect of sintering parameters on densification, microstructure and phases were tracked by DOE, and the effect of heat treatment on the phase was determined.

1. Introduction

Today, permanent magnets are among the most important advanced technological research topics because they are used in various application areas, such as transportation devices, biomedical devices, and electrical power generation devices, and their application areas are increasing [1].

Until recently, although permanent magnets have been produced from two main material classes, rare earth magnets (mostly Nd Fe-B) and hard ferrites, Al and Mn alternative materials have become an important focus of research due to their relative abundance, high-level energy production performance and low cost [2,3].

Hence, due to the unique properties mentioned, more than one study has been conducted on Mn-Al permanent magnets as an alternative to traditional permanent magnets, and there are publications in the literature.

Zeng et al. identified magnetism in the Mn-Al alloy system with the following statements. Mn metal is ordinarily antiferromagnetic. Mn becomes ferromagnetic by increasing the atomic distance. In the Mn-AI. system, a ferromagnetic phase can occur in the approximate composition range 51 < Mn < 58 at. %. This ferromagnetic phase has an ordered tetragonal $L1_0$ structure (c < a) in which manganese atoms are located at the (0,0,0) sites and coupled ferromagnetically. Aluminum atoms and manganese atoms in excess with respect to the equiatomicity enter (1/2, 1/2, 1/2) sites; Mn atoms in the two different sites are coupled antiferromagnetically. Fig. 1. Plots of two mechanisms have been proposed for τ-phase formation: hcp(ε) to B19(ε') and B19(ε') to fct(τ). In both mechanisms, the τ phase is formed by successive transformations; however, the usually accepted mechanism is that in which the high-temperature hexagonal-closed-packed structure (ε) transforms into an orthorhombic (ε') phase by an ordering

[1] ISTANBUL TECHNICAL UNIVERSITY, DEPARTMENT OF METALLURGICAL AND MATERIALS ENGINEERING, ISTANBUL, 34469, TURKEY

* Corresponding author. goller@itu.edu.tr

reaction and then to the metastable face-centered-tetragonal ferromagnetic τ phase in a martensitic mode. This metastable tetragonal τ AlMn phase possesses unit cell lattice parameters a = 3.54 Å and c = 3.92 Å. Since the minimum internal energy occurs very close to c/a = 1 (c and a are the lattice parameters), the tetragonal τ phase is reported to be metastable and is usually produced either by rapid quenching of the high-temperature ε-phase followed by isothermal annealing between 400 and 700°C or by cooling the ε-phase at a rate of 10°C/min. Prolonged annealing and elevated temperatures result in decomposition of the τ-phase into the equilibrium cubic Υ_2- and β-phases [4].

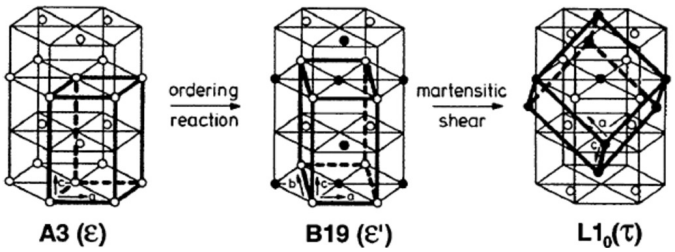

Fig. 1. Consecutive phase transformation steps a) first step hcp(ε) phase, b) second step B19(ε')phase, c) last step fct(τ) phase [5]

E. Fazakas et al. investigated the phase transformations on a nanocrystal $Mn_{54}Al_{44}C_2$ ribbon magnet sample obtained by melt spinning. According to this study, it was found that the metastable τ phase stabilized by carbon addition could be transformed reversibly into the ε-phase at approximately 800°C without decomposition into the stable Al_8Mn_5 and β manganese phases [6].

In another study, I.A. Radulov et al. prepared Mn-Al permanent magnets by using the electron beam melting method to obtain a fully dense structure and to focus on controlling the microstructure behavior during the electron beam melting process and the heat treatment process after manufacturing. In conclusion, this study found that the Al-Mn permanent magnets produced by EBM techniques contained 8% of the desired ferromagnetic τ MnAl phase and were fully dense. After all the samples were subjected to an optimized annealing treatment, the content of the τ phase increased to 90%. The sample had a coercivity value of 0.15 T, which is also the maximum achieved in conventionally produced binary MnAl magnets [2].

Shuang Zhao et al. synthesized $L1_0$ Mn-Al permanent magnet alloys by regulated heat treatment to determine the influence of substitutional atoms on intrinsic magnetic properties in $L1_0$ Mn-Al alloys. In this study, Co, which is used for $L1_0$, was found to degrade the stability of the phase, but the addition of Cu or Ga could stabilize it [7]. T. Mix et al. also worked on demonstrating the $L1_0$ structure produced in all ternary alloys of the form Mn55Al45-xGax. In alloys with 5 < x <9 at % Ga, we have shown that thermodynamically stable and metastable $L1_0$ phases can coexist, and different phase formation routes have been reported [8].

The spark-plasma sintering technique (SPS) was used to obtain anisotropic MnBi bulk magnets in the Yu-Chun Chen et al. study to investigate the microstructure effect of SPS-compacted MnBi magnets. According to this study, fast consolidation using SPS might be an effective method to modify the final material properties of sintered materials based on phase diagrams [9].

In another study, I. Janotova et al. produced binary Mn-Al and Mn-Bi magnetics by using the melt-spinning method and annealed it using diverse regimes to obtain the required phase composition and structure. The aim of this study was to show the joint effects of the alloying of constituent elements in binary Mn-Al and Mn-Bi together with the process of rapid quenching on the changes in physical properties caused by structural transformations. Several techniques were used to investigate the transformation to the ferromagnetic state and obtain the crystal structure. The results show that magnetic properties are directly affected by annealing regimes [10].

Van Tang Nguyen et al. synthesized $Mn_{55}Al_{45}$, $Mn_{55}Al_{44}C_1$, $Mn_{52.2}Al_{45.8}C_2$ and $Mn_{54.2}Al_{43.8}C_2$ by using a mechanical alloying method, which is different from a previous study, to show the purity of the τ phase and the effect and position of C doping on magnets. In this study, after 10 h of milling, annealing at 1050°C for 1 h and aging at 535°C for 45 minutes, the highest purity of the τ phase (99%) belonged to $Mn_{54.2}Al_{43.8}C_2$, and the other properties of these magnets were reported as $M_s = 570\ kAm^{-1}$, $M_r = 255\ kAm^{-1}$, $H_c = 143\ kAm^{-1}$ and $(BH)_{max} = 7.8\ kJ/m^3$. One of the important and different points of this study was that M_s is the highest value ever reported by the mechanical alloying method, and it could be said that carbon stabilizes the τ phase and reduces the magnetic moment of Mn [11]. There are similar studies in the literature regarding the investigation of τ phase changes with Mn-Al magnetic alloys that are carbon-doped. Shuang Zhao et al. investigated the effect of carbon addition on the $L1_0$ τ phase stability in $Mn_{0.54}Al_{0.46}$. In this study, the prepared magnet samples were annealed at high temperature, and the results show that the carbon-doped τ phase was also more stable, resulting in an obvious improvement in magnetization. The magnetization of 86.7 emu/g under 30 kOe and the coercivity of 3.26 kOe were approached in the as-annealed x = 3 powders. The best stability of the τ phase was obtained in the x = 3 alloy, and the τ phase was barely affected by heat treatment at 923°K for 25 h [12]. In another study, Le Feng et al. produced MnAl-C-Ni permanent magnets by extruding powders milled from a bulk material, which is a novel approach. As a result of this study, the materials produced using different conditions contained a large volume fraction (>0.92) of the desired τ phase [13].

The Taguchi method is a robust statistical tool for the design of high-quality systems. It uses control factors and noise factors, and with the combination of two, it enhances the design of the experiment [14]. The main aim of the Taguchi method is to optimize the settings of the process parameter values to improve the quality characteristics. The final step of the optimization is tolerance design, which is used to determine and analyze tolerances around the optimal settings recommended by the parameter design [15,16]. The scope of this paper is optimizing the sintering parameters (temperature, holding time and pressure) to reach the τ phase in a more efficient way.

2. Experimental procedures

Mn (H.C. Starck Corp.) and Al (H.C. Starck Corp.) powders were used as raw materials with 99.9% and 99.8% purity, respectively. Powders were evaluated with scanning electron microscopy. (SEM; Vega, Tescan). Particle size measurement of the powder was carried out by a laser particle sizer (Mastersizer 2000, Malvern Instruments). The powders were weighed in appropriate quantities, and then Mn (55% atomic percentage) and Al (45% atomic percentage) powders were mixed and ball milled (with 10:1 tungsten carbide balls) in ethanol for 24 h and dried. XRD analysis of the powder mixture was taken into consideration. The phase analyses of starting powder mixture was conducted by X-ray diffractometer (XRD; Panalytical Aeris) with Cu-Kα radiation. XRD analyses were carried out in the 2θ range of 10-90° and a step size of 0.02° in the step scan mode.

After preparation of the starting powder, a graphite die 50 mm in inner diameter was filled with the powder, followed by a sintering process using SPS equipment (SPS-7.40 MK-VII, SPS Syntex Inc.). The samples were sintered with the variable parameters of 700-800-900°C temperature, 60-300-600 second holding times and uniaxial pressures of 30-40-50 MPa (TABLE 1). Different sintering parameters, temperature, holding time and pressure, were selected according to the literature and dummy tests. In the phase diagram, 870°C was the phase transformation temperature. In dummy experiments, a sintering temperature of 850°C was manufactured, and the relative density was evaluated. An experimental design was used to reach the maximum relative density and minimum average grain size. Samples were produced according to the L9 Taguchi design. Three factors, sintering temperature, holding time and sintering pressure, were selected as 3 levels. A pulsed direct current (12 ms/on, 2 ms/off) was applied during the entire SPS process under a vacuum atmosphere. The die temperature was measured by an optical pyrometer (Chino, IR-AH), and sintering was conducted under temperature-controlled mode by monitoring the shrinkage behavior of the samples during the SPS process.

The bulk density of the sintered samples was determined by Archimedes' method and converted to relative density. Sample density was crosschecked with an X-ray Inspection Device (XRay, Nordson Dage, Quadra 3), and the amount of porosity was evaluated. The microstructural characterization was determined by scanning electron microscopy after the sample preparation procedure. Elemental analysis was evaluated with energy dispersive spectroscopy (EDS). Grain boundaries were observed after etching with Keller Reagent (2.5 ml HNO_3, 1.5 ml HCl, 1.0 ml HF, and 95 ml H_2O). The average grain sizes were calculated using the linear interception method (ASTM E112-13). Heat treatment was carried out with a Nabertherm muffle furnace Model P 320. Within this work, Mn-Al alloy samples were heated between 450-650°C, which was higher than the phase transformation temperature of the pure alloy, and cooled at ambient temperature (air) or water quenched. Samples were held for 60 minutes. After the heat treatment process, differences in the microstructure and crystalline structure were observed. The phase analyses of sintered samples were conducted by X-ray diffractometer (XRD; Panalytical Aeris) with Cu-Kα radiation. XRD analyses were carried out in the 2θ range of 10-90° and a step size of 0.02° in the step scan mode.

Magnetic properties were evaluated with a vibrating sample magnetometer (VSM). VSM support was provided by Dokuz Eylul University. A Dexing Magnet VSM 550 was used in this study. The scope of measured magnetic moment was between 10-2emu–300emu and scope of measured magnetic field was between 0 to 3.5T. Solid sintered samples were compared with each other.

3. Results and discussion

a. Starting powder properties (particle size, xrd, sem/eds)

The average particle sizes of the Mn and Al powders (d90) were 23.6 and 258.4 μm, respectively. On the other hand, the average particle size of the Mn-Al mixture (d90) was 161.667 μm. Particle size distribution graphs are given in Fig. 2.

TABLE 1

Temperatures, holding times; pressures, relative densities, average grain sizes and magnetic properties of SPS'ed samples

Code#	DOE#	Sintering Temperature (°C)	Holding Time (Second)	Sintering Pressure (MPa)	Calculated Density (g/cm^3)	Relative Density (%)	Average Grain Size (μm)	ASTM Number #
N1	111	700	60	30	4.4046	83%	158.4 ±17.8	2.04
N2	122	700	300	40	4.8402	91%	116.6±10.7	2.9
N3	133	700	600	50	5.0815	95%	169.2±22.5	1.86
N4	212	800	60	40	5.0916	96%	178.1±31.8	1.73
N5	223	800	300	50	5.0345	94%	223.4±35.7	1.06
N6	231	800	600	30	5.2419	99%	137±18.1	2.49
N7	313	900	60	50	5.1222	96%	312.5±86.3	0.16
N8	321	900	300	30	4.9823	94%	213.1±27.4	1.2
N9	332	900	600	40	4.8602	91%	125.2±38.2	2.82

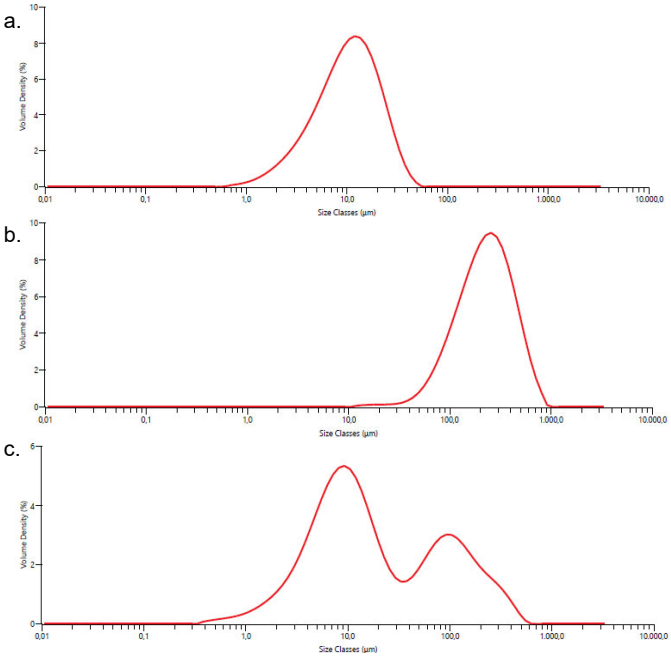

Fig. 2. Particle size distributions of (a) Mn, (b) Al, (c) Mn-Al mixture

The SEM observations shown in Fig. 3 reveal the morphology of the starting powders. Elemental analyses from several points were taken, and it was understood that the compositions of these points are Spot 1 Mn-Al 52.3% & 47.7% and Spot 2 Mn-Al 59.13% & 40.87%, (weight percentages).

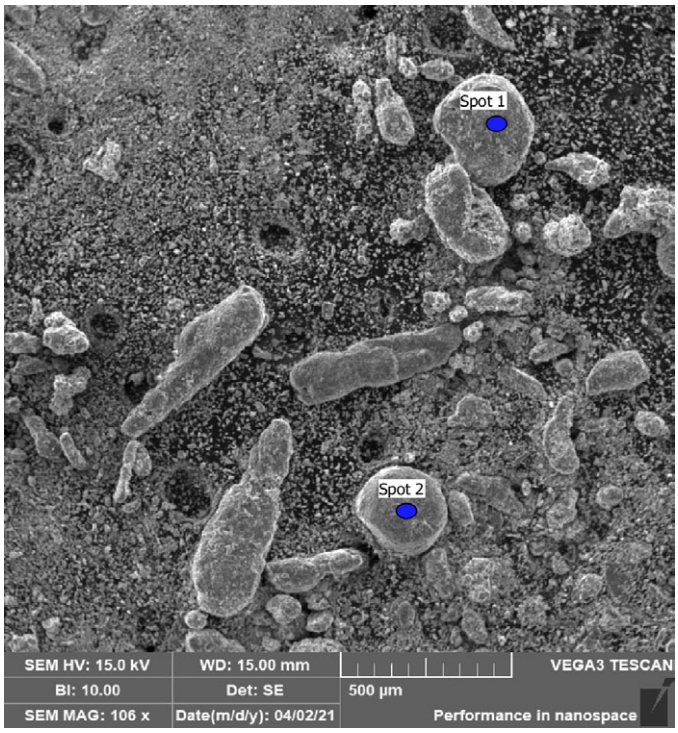

Fig. 3. Morphology of starting powder mixture and EDS spot 1 and spot 2

The phases of the starting powders were determined and are given in Fig. 4. In addition, characteristic peaks of Mn (ICDD: 00−001-1237) and Al (ICDD: 00−003-0932) were detected in the XRD pattern. Mixtures of starting powders were evaluated, and it was checked whether there was any contamination.

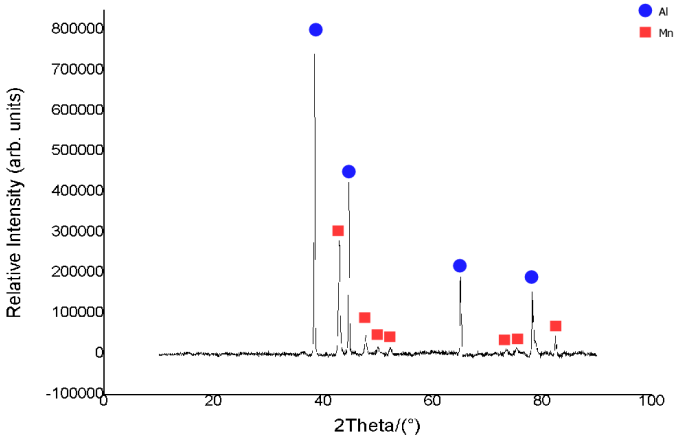

Fig. 4. XRD patterns of starting powders Mn-Al

b. Densification behavior & Xray

The calculated density and relative density values are given in TABLE 1. The theoretical density of Mn-Al samples was considered to be 5.3 g/cm^3. Calculations were carried out according to samples that were produced 50 mm in diameter and 4 mm thick.

Relative density values were also crosschecked with X-ray (nondestructive) imaging, which is shown in Fig. 5. According to X-ray images, porosities were observed in some samples. Slightly lighter areas indicate lower density. These results are compatible with the relative density values. Least dense sample N1 Fig. 5(a). has a larger porous area and the highest density in sample N6 (Fig. 5(f)). has the smallest porous area.

The effects of the sintering temperature, holding time and pressure on the relative density values were investigated. These investigations were conducted statistically with the help of the Taguchi Design of Experiment. In the scope of this work, it was assumed that denser materials demonstrate higher magnetic properties. According to this assumption, one of the aims of this study is to obtain denser materials. 'Larger is better' was selected as the signal-to-noise proportion, and according to this estimation, the relationship between sintering parameters (sintering temperature, holding time and sintering pressure) and densification is shown in Fig. 6. According to the Taguchi prediction, the highest density could be obtained at 800°C, 600 sec, and 50 MPa. The regression equation and model summary are also added below.

Regression Equation

Density = –0.489 + 0.001446 Temp + 0.001411 Time + 0.0315 Pres. – 0.000001 Temp * Time – 0.000031 Temp * Pres. – 0.000019 Time * Pres.

Model Summary

S	R-sq	R-sq(adj)	R-sq(pred)
0.03	88.71%	54.83%	0.00

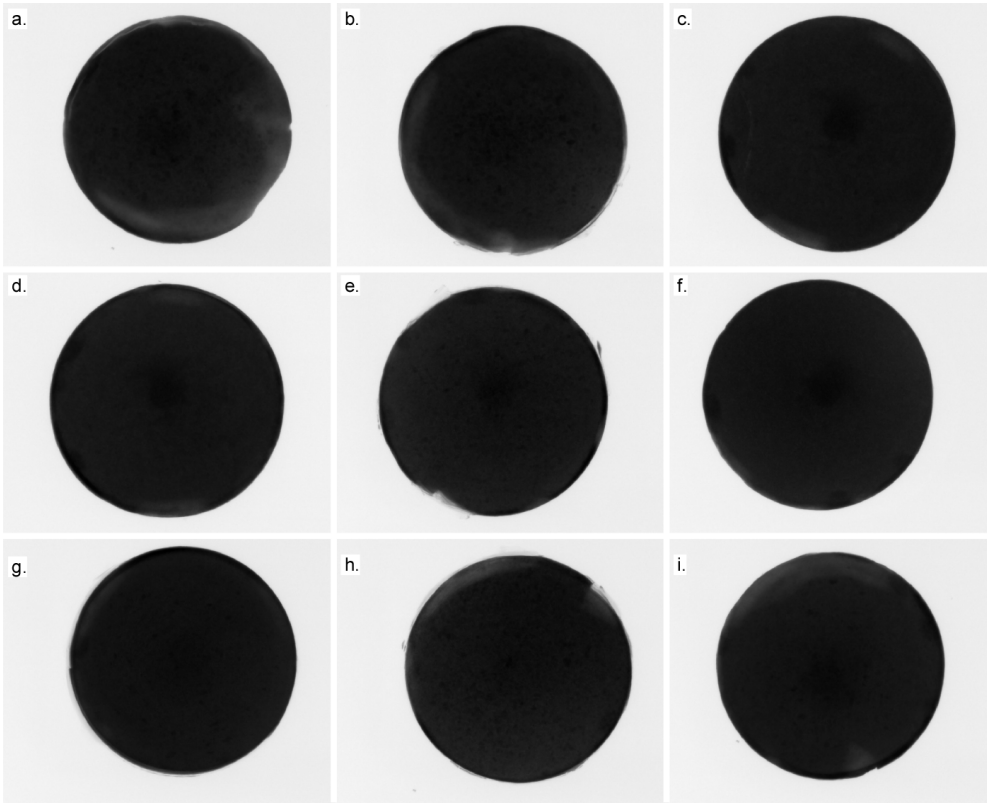

Fig. 5. Xray images of sintered Mn-Al samples (a) N1, (b) N2, (c) N3, (d) N4, (e) N5, (f) N6, (g) N7, (h) N8, (i) N9

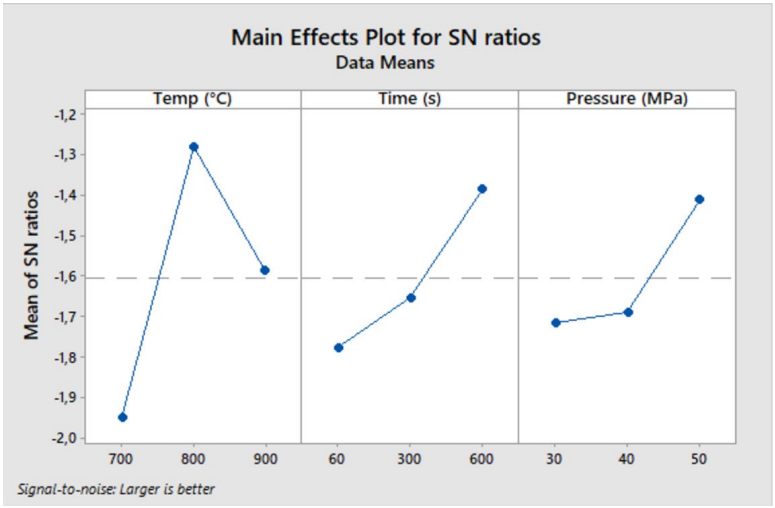

Fig. 6. Main Effects Plot of Sintering parameters on relative density

c. Microstructural observation (average grain size)

Average grain sizes were calculated with the linear interception method, and the results are given in TABLE 1. According to optical images of etched samples, the smallest grain-sized sample is N2 (116.6±10.7 µm), and the largest grain-sized sample is N7 (312.5±86.3 µm). Overall etched images can be seen in Fig. 7.

The sintering temperature, holding time and pressure effects on grain size were investigated. These investigations were conducted statistically with the help of the Taguchi Design of Experiment. In the scope of this work, it was assumed that the smallest grain-sized materials demonstrate higher magnetic properties. According to the Hall-Petch equation, mechanical properties are affected by grain size. According to this assumption, one of the aims of this study is to investigate the effects of grain size on magnetic properties. When reaching the smallest grain size, the material shows higher magnetic properties. 'Smallest is better' was selected as the signal-to-noise proportion, and according to this estimation, the relationship between sintering parameters (sintering temperature, holding time and sintering pressure) and densification is shown in Fig. 8. According to the Taguchi prediction, the smallest grain size was obtained at 700°C, 600 sec, and 40 MPa. The regression equation and model summary are also added below.

Regression Equation

Average Grain Size = 315 – 0,01 Temp +
1.345 Time – 26.2 Pres. – 0.00223 Temp *
Time + 0,0296 Temp * Pres. + 0.0089 Time * Pres.

Model Summary

S	R-sq	R-sq(adj)	R-sq(pred)
38.4078	90.16%	60.63%	0.00%

Scanning electron images of all samples with (seconder electron and back scattered electron mode) were gathered (shared at Fig. 9. Fig. 10. At Fig. 10. No other phases except Mn-Al were found. Elemental analyses of several points were applied, and it was understood that the compositions of these points are Spot 1 Mn-Al 52.3% and 47.7% and Spot 2 Mn-Al 59.13% and 40.87%, respectively. Therefore, the lighter gray area was richer in Mn, and the darker area was richer in Al.

d. Crystalline phase analyses

The crystalline phases of the sintered samples were determined and are given in Fig. 11. The X-ray diffractometer was used for phase identification of sintered samples (n1-n9) in the 2θ range of 10-75°. The main aim of this XRD study is to understand whether the sintered samples formed the τ phase. However, during analysis, a related phase was not found. The characteristic peaks of the τ phase are ICDD: 00−030-0028, the stoichiometric formula is $Al_{0,89}Mn_{1,11}$ and the bravia lattice

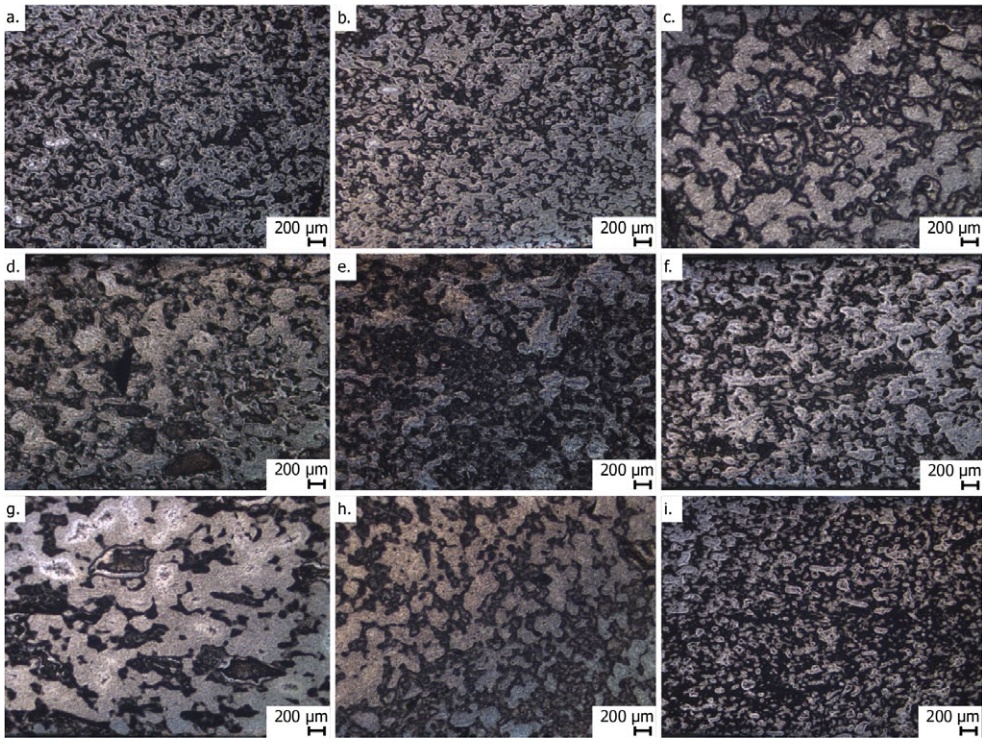

Fig. 7. Optical images of etched Mn-Al samples (a) N1, (b) N2, (c) N3, (d) N4, (e) N5, (f) N6, (g) N7, (h) N8, (i) N9

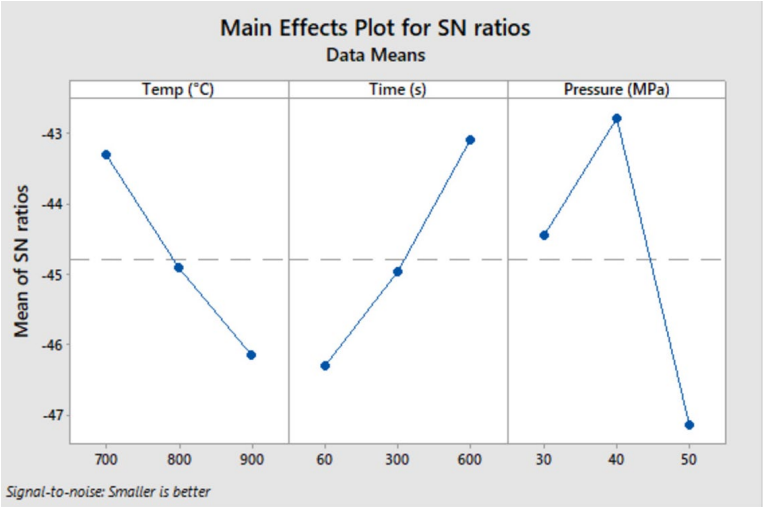

Fig. 8. Main Effects Plot of Sintering parameters on average grain size

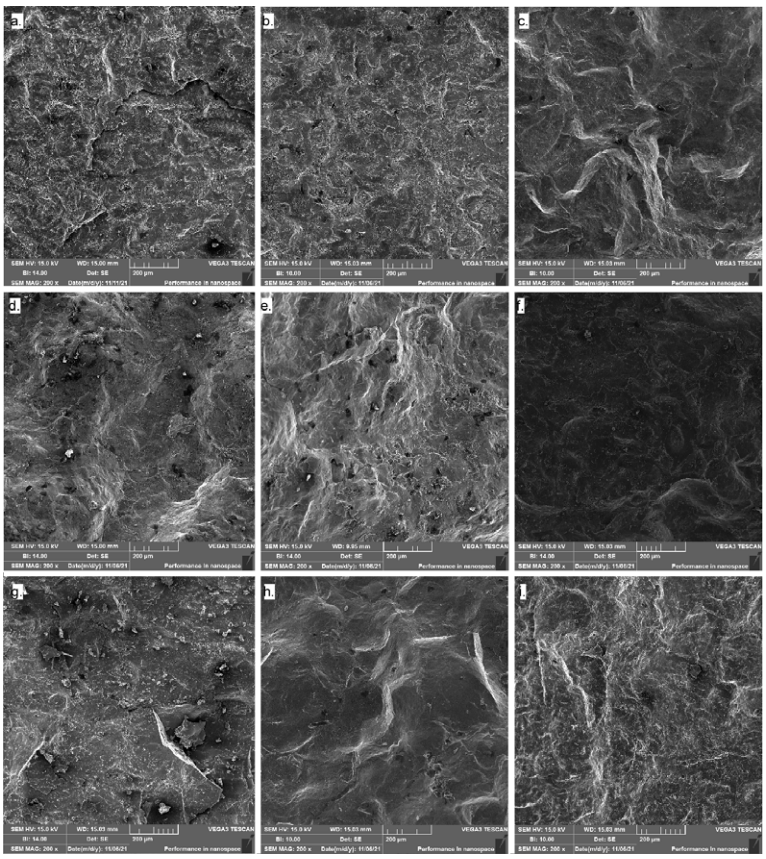

Fig. 9. Scanning electron microscope (Seconder) images of etched Mn-Al samples (a) N1, (b) N2, (c) N3, (d) N4, (e) N5, (f) N6, (g) N7, (h) N8, (i) N9

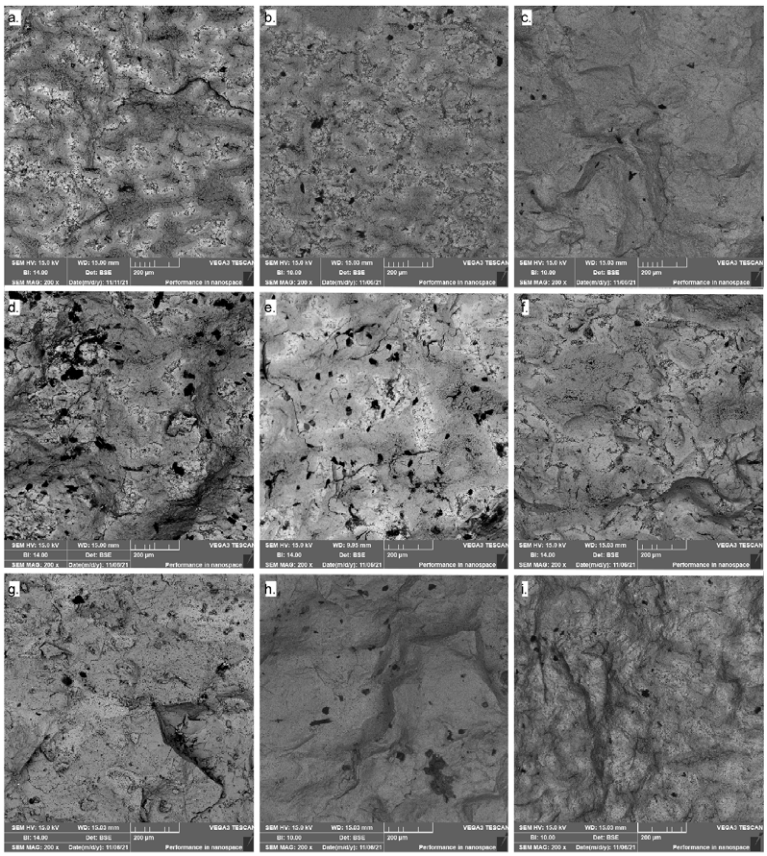

Fig. 10. Scanning electron microscope (back scatter) images of etched Mn-Al samples (a) N1, (b) N2, (c) N3, (d) N4, (e) N5, (f) N6, (g) N7, (h) N8, (i) N9

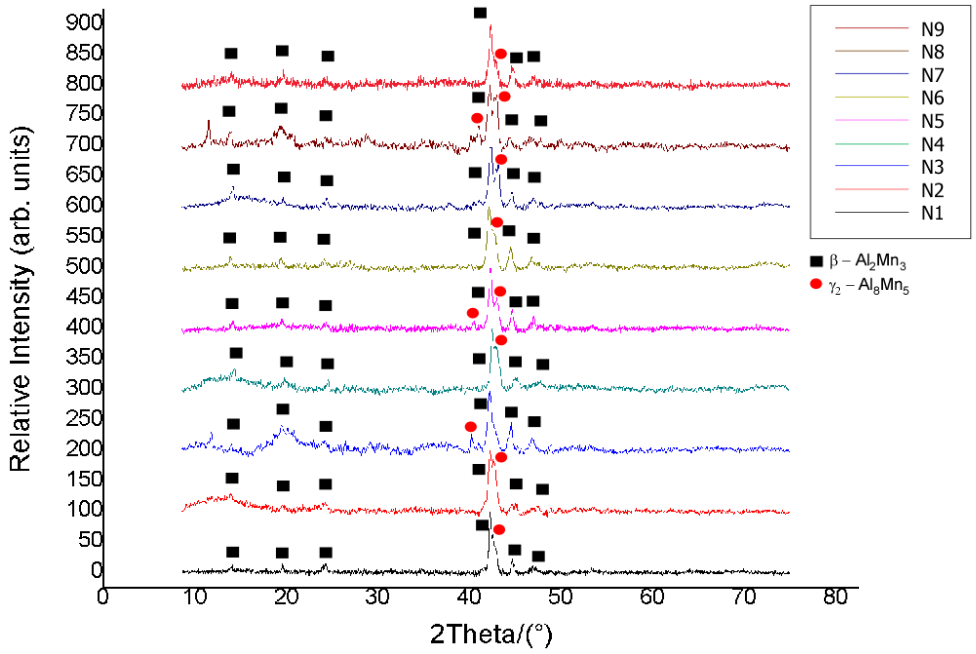

Fig. 11. Xrd patterns of Mn-Al sintered samples (a) N1, (b) N2, (c) N3, (d) N4, (e) N5, (f) N6, (g) N7, (h) N8, (i) N9

is tetragonal. At patterns, β and γ_2 phases were found. Characteristic β (ICDD: 00−048-1568) and γ_2 (ICDD: 00−018-0035) peaks were detected in the XRD pattern (Fig. 11). Nguyen et al. mentioned that the stoichiometric formula of the β phase is Al_2Mn_3 and the γ_2 phase is Al_8Mn_5, and the bravia lattices are cubic and rhombohedral. [11]

e. Heat treatment

In the XRD studies, it was understood that the τ phase was not achieved. To reach the τ phase, several heat treatments were tried. The N6 sample was selected, and heat treatment was applied to this sample because the density of 6 is higher and the average grain size of this sample is tolerable. Four different heat treatments were applied to the N6 sample. During the first heat treatment, the sample was heated to 450°C in a furnace at 10°C/min, kept at 450°C for 45 minutes and directly quenched with water. Second, the sample was heated to 450°C in a furnace at 10°C/min, kept at 450°C for 45 minutes and cooled in an air atmosphere. Third, the sample was heated to 650°C in a furnace at 10°C/min, kept at 650°C for 65 minutes and directly quenched with water. Finally, the sample was heated to 650°C in a furnace at 10°C/min, kept at 650°C for 65 minutes and cooled to ambient temperature (air atmosphere). Details of the heating regimes can be found in Fig. 12. 450-650°C temperature selected based on Palanisamy et al.'s study [17].

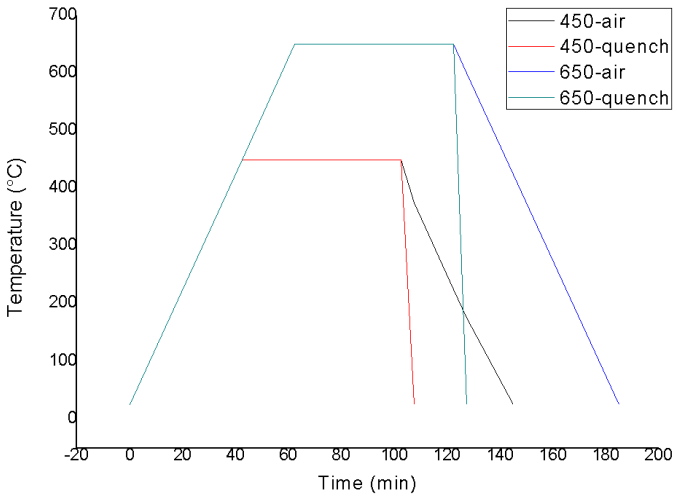

Fig. 12. Several heat treatment applied to N6. (a) 450-air, (b) 450-quench, (c) 650-air, (d) 650-quench

After heat treatments, XRD analysis was reapplied to the samples. The phases of the heat-treated samples were determined and are given in Fig. 13. Both samples were heated to 450°C but cooled in a different way; however, both showed the same characteristics. For those two samples, the target phase (τ) could not be reached. Nevertheless, at both heat treatments heated to 650°C, different peaks were obtained. When these different peaks were investigated deeply, these peaks were not β and γ_2 phases. These peaks were similar to the characteristic peaks of the τ phase, which is ICDD: 00−030-0028.

Scanning electron microscopy of heat-treated samples (N6-650 quenched) was investigated, and elemental analyses were conducted (Fig. 14). Elemental analyses of several points were taken, and it was understood that the compositions of these points are Spot 1 Mn-Al 50.35% & 49.65% and Spot 2 Mn-Al 56.95% & 43.05%, (weight percentages). In these images, similar structures (with Wei et al.) were found [18]. It was suggested that these structures were τ phase. According to the Sem analyses in Fig. 14. the τ phase could not be clearly detected. To understand more about the τ phase, the magnetic properties of heat-treated samples were checked with a vibrating sample magnetometer.

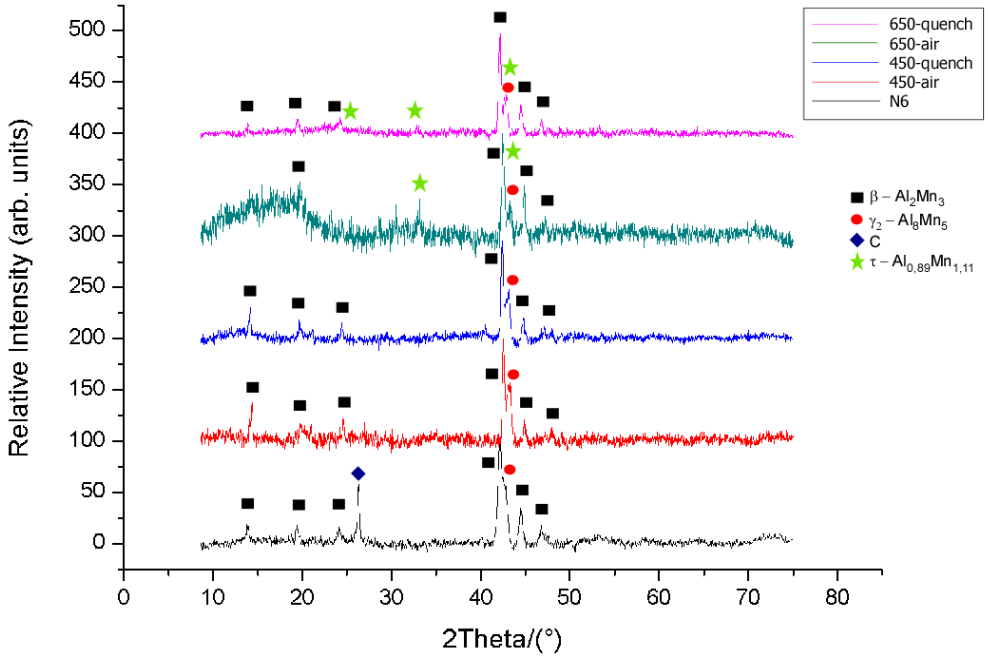

Fig. 13. Xrd patterns of heat treated Mn-Al sintered samples (a) ref N6, (b) 450-air, (c) 450-quench, (d) 650-air, (e) 650-quench

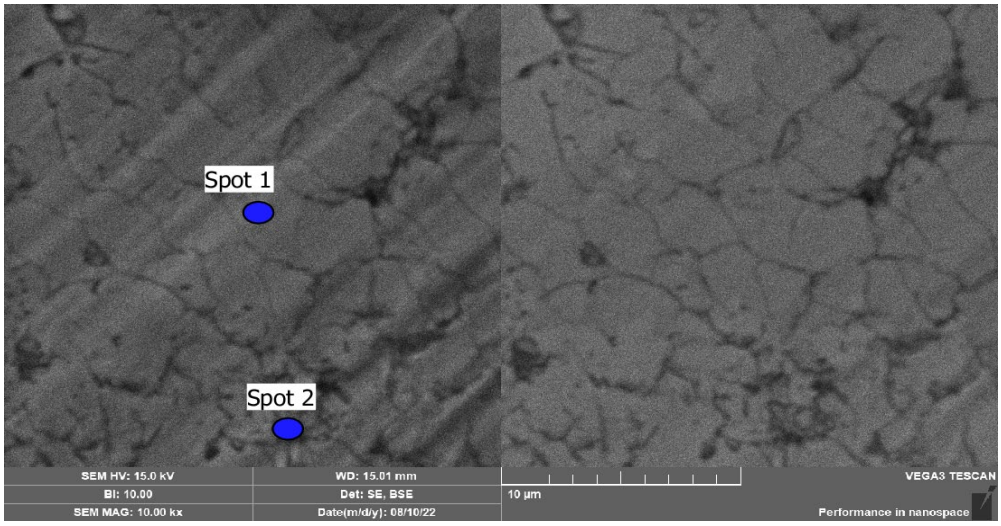

Fig. 14. Scanning electron microscope images of N6 650-quenched Mn-Al samples (a) SE, (b) BSE

f. Magnetic properties

TABLE 2

Effects of various heat treatments on magnetic properties of SPS'ed samples

Ref Sample	Heat Treatment	H_c (kA/m)	Saturation M_s (T)	Remanence M_r (T)
N6	—	22	0.217	0.853
N6	450-air	30	0.179	0.592
N6	450-quech	69	0.264	0.686
N6	650-air	69	0.543	1.293
N6	650-quech	22	0.217	0.853

Magnetic properties, which were evaluated with a vibrating sample magnetometer of sintered samples, were determined and are given in TABLE 2. Although no τ phase was observed in the samples after SPS, there was a significant increase in magnetic properties after heat treatment. As a result, it is clear that the SPS process is insufficient to obtain the τ phase and thus high magnetic properties and that heat treatment is needed. P. Saravanan et al., 2014, reported a similar result of not observing the τ phase on SPSed Mn-Al alloys (at two samples out of three in the article mentioned) [19].

The hysteresis curves of N6 samples ((a) ref N6, (b) 450-air, (c) 450-quench, (d) 650-air, (e) 650-quench) were given in Fig. 15. Although all VSM analyses were conducted at ambient temperature, according to the results of the measurements, N6 heat treated with 650 air demonstrated the best magnetic properties among the heat treatment parameters. This significant improvement seen in the 650 air heat treatment

can be caused by the time needed for diffusion to cool and reach stable phases.

Before heat treatment, coercive force (H_c) value of reference sample N6 is 22 kA/m. After 450-air, 450-quench, 650-air and 650-quench heat treatments, the values were 30,69,69 and 22 kA/m, respectively. According to results 450-quench and 650-air showed best coercivity which is a measure of the ability of a material to withstand an external magnetic field without becoming demagnetized.

The measured magnetization of saturation (M_s) value of reference sample N6 increased significantly after the 650-air heat treatment. The M_s value without any heat treatments is 0.217 T. M_s values after the 450-air, 450-quench, 650-air, and 650-quench heat treatments were 0.179, 0.264, 0.543 and 0.217 respectively. The M_s values are compatible with the samples obtained by Liu et al. [20]. Also Saravanan et al. mentioned at relatively lower temperatures, the weight percent of the obtained τ phase is lower, as mentioned in an article that compares the τ phase observation at different annealing temperatures and explains the fact that at 500-700°C, it shows less than 1 Am^2/kg M_s values even with the carbon-added samples, and the increase in M_s indicates an increase in the τ phase during heat treatment [19]. In addition the highest remanence (M_r) value is also observed in the sample treated with 650-air.

In summary, the measurement results indicate that with the 650-air heat treatment, the magnetizing force, saturation, retentivity and loop area increased. Hence, the appropriate heat treatment method among the other methods mentioned in this experiment is 650-air. The magnetic property values of the

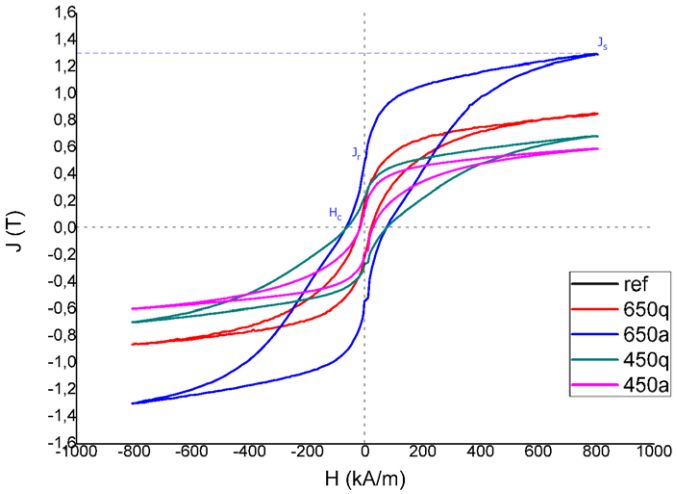

Fig. 15. Hysteresis curves of N6 (a) ref N6, (b) 450-air, (c) 450-quench, (d) 650-air, (e) 650-quench

SPSed and 650-air heat treated Mn-Al sample are similar with the magnetic property values of similarly processed Mn-Al samples obtained by Liu et al. By enhancing the fraction of the τ phase by optimizing the heat treatment process by increasing the temperature and adding a small amount of carbon, the Mn-Al samples made in this research can further improve their magnetic characteristics.

Finally, the effects of heat treatment temperature and cooling methods on magnetization were investigated. These investigations were conducted statistically with the help of the Taguchi Design of Experiment. L4 'Larger is better' was

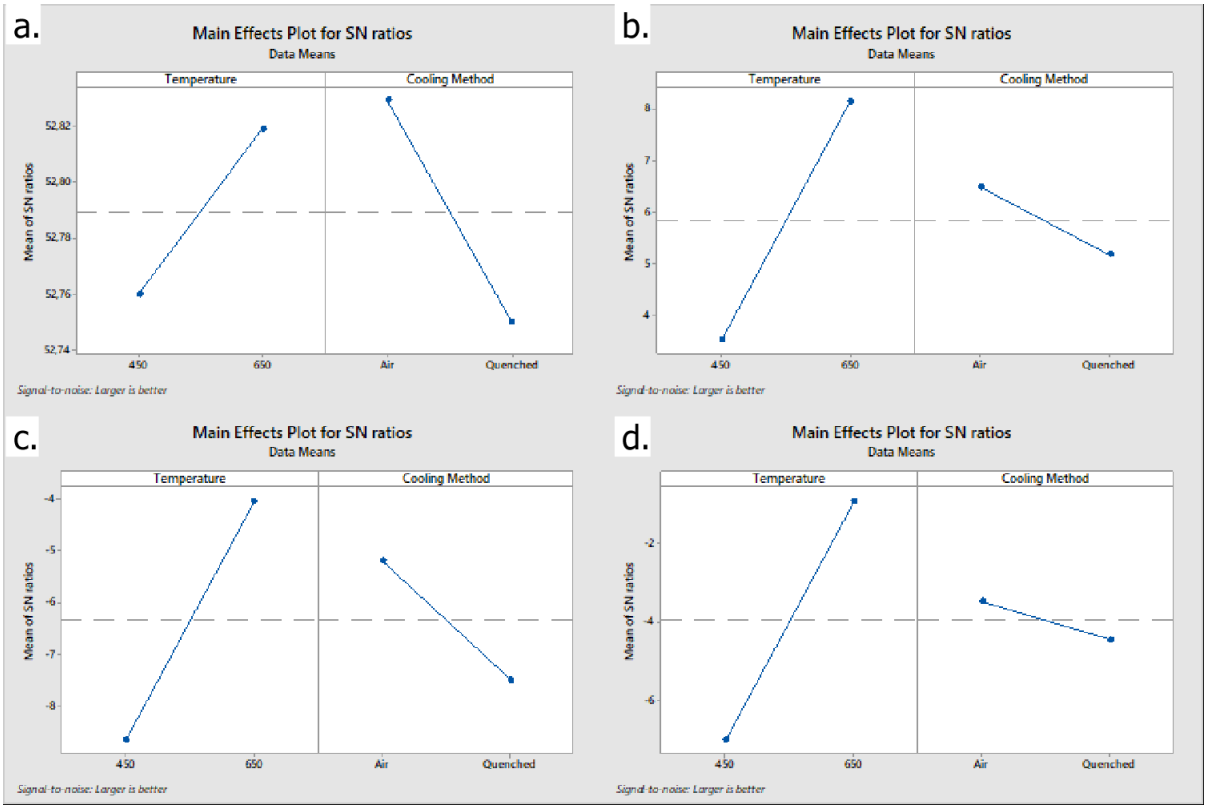

Fig. 16. Main effects plot of heat treatment parameters on magnetization (a) Magnetic force, (b) Saturation, (c) Remanence, (d) Loop area

selected as the signal-to-noise proportion, and according to this estimation, the relationship between heat treatment conditions and magnetization is shown in Fig. 16. It was understood that 650-air demonstrates the best magnetic properties. Since the cooling method (air/quench) uses discrete data, Taguchi prediction could not be performed.

4. Conclusion

In this study, Mn-Al alloys were produced by SPS, and the effects of sintering parameters on density, grain size and magnetic properties were investigated. In conclusion, the highest density values reached 5.24 g/cm^3, with a relative density of 99% (N6 800°C – 600 s – 30 MPa). This N6 sample's grain size is 137 µm. The effects of sintering parameters on densification, microstructure and phases were tracked by DOE. Denser material and lower grain-sized samples were produced with the help of DOE. This study is a great example to demonstrate the power of DOE because the purpose of DOE is to optimize the process. With minimum sample size, statistical calculations supported the manuscript. However, samples with magnetic properties could not be produced with SPS in the first trial. Reaching the τ phase occurred with the help of heat treatment. The direct relationship between magnetic properties, grain size and density has been explained in this paper. Nonetheless, the most active parameter for magnetic properties is the phase. To reach the specific phase, several heat treatments were applied to the samples. The sample that was heated to 650°C and cooled to ambient temperature showed magnetic properties.

Acknowledgement

The authors thank Asst. Prof. Dr.Nuri Solak for his contribution for XRD studies, Dr. Burak Cagri Ocak in SPS studies, Eymen Konyali and Bengi Su Yilmaz for their support.

REFERENCES

[1] D.P. Hoydick, E.J. Palmiere, W.A. Soffa, On the formation of the metastable llo phase in manganese-aluminum-base permanent magnet materials **36**, 2, 151-156 (1997).

[2] I.A. Radulov et al., Production of net-shape Mn-Al permanent magnets by electron beam melting, Addit. Manuf. **30**, 100787 (2019).

[3] S.F. Marenkin, A. Ril, Al – Mn Hard Magnetic Alloys as Promising Materials for Permanent Magnets Al – Mn Hard Magnetic Alloys as Promising Materials for Permanent Magnets (Review), no. October, 2021.

[4] Q. Zeng, I. Baker, J.B. Cui, Z.C. Yan, Structural and magnetic properties of nanostructured Mn – Al – C magnetic materials **308**, 214-226 (2007).

[5] J.J. Van Den Broek, H. Donkersloot, G. Van Tendeloo, J. Van Landuyt, Phase transformations in pure and carbon-doped Al45Mn55 alloys, Acta Metall. **27**, 9, 1497-1504 (1979).

[6] E. Fazakas, L.K. Varga, F. Mazaleyrat, Preparation of nanocrystalline Mn – Al – C magnets by melt spinning and subsequent heat treatments **435**, 611-613 (2007).

[7] S. Zhao, Y. Wu, J. Zhy, Y. Jia, Evolution of Intrinsic Magnetic Properties in L10 Mn − Al Alloys Doped with Substitutional Atoms and Correlated Mechanism : Experimental and Theoretical Studies Evolution of Intrinsic Magnetic Properties in L1 0 Mn-Al Alloys Doped with Substitutional Atoms and Correlated Mechanism : Experimental and Theoretical, no. June, 2019.

[8] T. Mix, F. Bittner, K. Müller, L. Schultz, T.G. Woodcock, Acta Materialia Alloying with a few atomic percent of Ga makes MnAl thermodynamically stable **128**, 160-165 (2017).

[9] Y. Chen et al., Magnetic and microstructural properties of anisotropic MnBi magnets compacted by spark plasma sintering, J. Alloys Compd. **830**, 154605 (2020).

[10] I. Janotová et al., Formation of magnetic phases in rapidly quenched Mn-Based systems, J. Alloys Compd. **749**, 1, 128-133 (2018).

[11] V. Tang Nguyen, F. Calvayrac, A. Bajorek, N. Randrianantoandro, Mechanical alloying and theoretical studies of MnAl(C) magnets, J. Magn. Magn. Mater. **462**, C, 96-104 (2018).

[12] S. Zhao et al., Stabilization of τ-phase in carbon-doped MnAl magnetic alloys, J. Alloys Compd. **755**, 257-264 (2018).

[13] L. Feng, J. Freudenberger, T. Mix, K. Nielsch, T. George, Acta Materialia Rare-earth-free MnAl-C-Ni permanent magnets produced by extrusion of powder milled from bulk, Acta Mater. **199**, 155-168 (2020).

[14] T. Sivaprakasam, Analyses of surface roughness by turning process using Taguchi method, January, 2007.

[15] N. Raghunath, P.M.P. Ã, Improving accuracy through shrinkage modelling by using Taguchi method in selective laser sintering **47**, 985-995 (2007).

[16] N. Kumar, H. Kumar, J. Singh, Experimental Investigation of process parameters for rapid prototyping technique (Selective Laser Sintering) to enhance the part quality of prototype by Taguchi method **23**, 352-360 (2016).

[17] D. Palanisamy, C. Srivastava, G. Madras, K. Chattopadhyay, High-temperature transformation pathways for metastable ferromagnetic binary Heusler (Al – 55 at .% Mn) alloy, J. Mter. Sci. **52**, 7, 4109-4119 (2017).

[18] J.B.Y.J.Z. Wei, Z.G. Song, Y.B. Yang, S.Q. Liu, H.L. Du, J.Z. Han, D. Zhou, C.S. Wang, Y.C. Yang, A. Franz, D. Többens, τ- MnAl with high coercivity and saturation magnetization 127113, no. December 2014.

[19] P. Saravanan, V.T.P. Vinod, Č. Miroslav, A. Selvapriya, D. Chakravarty, S.V. Kamat, Processing of Mn – Al nanostructured magnets by spark plasma sintering and subsequent rapid thermal annealing, J. Magn. Magn. Mater. **374**, 427-432 (2015).

[20] Z.W. Liu, C. Chen, Z.G. Zheng, B.H. Tan, R.V Ramanujan, Phase transitions and hard magnetic properties for rapidly solidified MnAl alloys doped with C , B, and rare earth elements, 2333-2338 (2012).